A column generation heuristic for VMAT planning with adaptive CVaR constraints

Pınar Dursun[1], Z. Caner Taşkın[1], İ. Kuban Altınel[1], Hatice Bilge[2], Nazmiye Dönmez Kesen[2], Murat Okutan[2], Ethem Nezih Oral[2]

[1] Department of Industrial Engineering, Boğaziçi University, 34342, Bebek, İstanbul, Turkey
[2] Institute of Oncology, İstanbul University, 34093, Fatih, Çapa, İstanbul, Turkey

E-mail: altinel@boun.edu.tr, pinar.dursun@boun.edu.tr, caner.taskin@boun.edu.tr, hbilge@istanbul.edu.tr, nazmiye.kesen@istanbul.edu.tr, mokutan@istanbul.edu.tr, enoral@istanbul.edu.tr

Abstract.

In this study we develop an efficient computational procedure that generates medically acceptable treatment plans for volumetric modulated arc therapy with constant gantry speed. Our proposed method is a column generation heuristic based on a mixed integer linear programming model, where the objective function contains minimization of total monitor unit of the treatment plan and dose-volume requirements are included as conditional value-at-risk constraints. Our heuristic generates a full treatment arc for the restricted master problem and calibrates the right hand side parameters of the conditional value-at-risk constraints in the first phase. In the second phase, this initial solution is improved by performing column generation. This is a fully automated procedure and produces treatment plans in a single call without any human intervention. We evaluate its performance on real prostate cancer data by comparing the quality of the generated plans with those obtained by a widely used commercial treatment planning system. Our analysis shows that the results are promising, and the generated plans satisfy the prescription restrictions and require 22% fewer monitor units on average compared to the ones obtained using Eclipse.

Keywords: VMAT, column generation, constant gantry speed, shortest path problem, prostate cancer, real clinical data sets

Submitted to: *Phys. Med. Biol.*

1. Introduction

Volumetric modulated arc therapy (VMAT) is a state-of-the-art modality of external-beam radiation, in which the gantry of the linear accelerator rotates around the body along one or more arcs and delivers radiation continuously. During the rotation, the radiation beam is shaped by a multileaf collimator (MLC) system made up of a number of parallel movable metal leaf pairs and mounted on the linear accelerator. Furthermore, dose rate and gantry speed can change simultaneously while the gantry is rotating. These features of VMAT enable it to produce radiation therapy plans having high conformal dose distributions with fewer monitor units (MUs) compared to intensity modulated radiation therapy (IMRT) (Teoh et al. 2011, Cambazard et al. 2012). Also, radiation delivery times of the resulting plans are significantly shorter. However, total MUs of VMAT and IMRT plans are higher compared to conventional three-dimensional conformal radiation therapy (3D-CRT) (Palma et al. 2008, Teoh et al. 2011). It is known that higher MU means higher integral body dose and higher risk of secondary malignancy as a result (Hall & Wuu 2003). To this end, we focus on finding the VMAT plans that are not only feasible with respect to clinical prescriptions, but also require fewer MUs compared to the existing methods in a reasonable amount of computation time.

VMAT planning is a challenging issue in radiation therapy due to the unique characteristic of the technique that causes additional constraints and makes the problem much harder compared to IMRT. The leaves of MLC can move and shape the beam during rotation, but there is a limitation on the speed of this movement: the beam shapes (apertures) at two consecutive beam angles (control points) must be compatible in terms of maximum leaf motion limitation, namely they are interdependent. This requires considering all apertures on a full treatment arc (360° arc) together. VMAT planning models yield large-scale formulations due to these properties of the technique. Another important issue in VMAT planning is to take into account dose-volume constraints of target volumes (TVs) and organs at risk (OARs). In the literature, there are different ways to formulate these constraints. In the first and widely applied approach, a nonlinear and volume-sensitive penalty term is added to the objective function. In another approach, a set of binary decision variables (one for each voxel) is included to the model and used to determine the fraction of the voxels in a structure that satisfy the dose limit. Unfortunately, this leads to a large-scale mixed integer linear programming (MILP) model, which is computationally difficult to solve for most clinical cases. The use of conditional value-at-risk (CVaR) constraints (Rockafellar et al. 2000) is a more promising way that does not require additional integer variables and yields more reasonable formulations in terms of computational cost. In this approach, the average dose in the upper (or lower) tail of an OAR's (or TV's) dose distribution is forced to satisfy the corresponding dose objective. However, CVaR functions result in very tight dose-volume constraints, which makes it much harder to obtain feasible plans. For all these reasons, most of the models in the literature are not comprehensive enough to take all aspects of VMAT treatment into account (i.e. not all of the dose prescriptions for every structure are explicitly considered in the formulation) due to increasing computational difficulty.

VMAT is not the first radiation treatment technique that benefits from the flexibility a rotating gantry introduces in order to obtain treatment plans with higher quality. Yu (1995)

proposed the rotational IMRT called intensity modulated arc therapy (IMAT); but the clinical implementations remained very limited until Otto (2008) suggested VMAT. In VMAT, the gantry speed and the dose rate as well as the beam shape can vary during rotation. There are two main VMAT planning approaches in the literature. In the first one, a two-step algorithm is used to convert an idealized IMRT plan consisting of fluence maps at both coarse (Luan et al. 2008, Wang et al. 2008, Cao et al. 2009) and dense (Craft et al. 2012, Wala et al. 2012, Salari et al. 2012) sampling of control points into a deliverable VMAT plan. Direct aperture optimization (DAO) is the second approach in VMAT planning, where beam shapes (i.e. aperture shapes or leaf positions) and beam intensities at all control points are optimized simultaneously. Otto (2008) and Yan et al. (2018) start with a coarse sampling of the control points and use heuristic methods to find the final VMAT treatment plan. Bzdusek et al. (2009) and Bedford (2009) propose a three-step framework where they find initial apertures at the first two steps, then they refine them in the third step where aperture shapes and intensities are the decision variables. Christiansen et al. (2018) modify the algorithm of Bzdusek et al. (2009) in order to make the continuous aperture dose calculation possible. Men et al. (2010) and Peng et al. (2012) propose a column generation based heuristic to solve a large-scale convex programming problems. Mahnam et al. (2017) develop a large-scale nonlinear integer programming model that minimizes a quadratic voxel-based least square penalty function. Their model optimizes the gantry speed in addition to the leaf positions and the dose rate at each control point. They also propose a column generation heuristic, where the subset of sequential apertures (i.e. the partial arcs) are considered as columns in their formulation. In their recent work, Mahnam et al. (2019) integrate DVH criteria into their column generation heuristic. Peng et al. (2015) propose a heuristic approach to solve VMAT with constant gantry speed and dose rate. In addition to constant gantry speed and dose rate assumptions, Papp & Unkelbach (2014) formulate the problem in such a way that MLC leaves move unidirectionally over an arc segment. On the other hand, Hoegele et al. (2012) optimize leaf motion by utilizing a *priori* knowledge about the type of the leaf motion pattern during delivery. Gozbasi (2010), Akartunalı et al. (2015), and Song et al. (2015) formulate large-scale MILP models for the problem. Gozbasi (2010) and Song et al. (2015) relax some treatment related constraints and aim to satisfy them via the objective function (e.g. minimizing total deviation from the prescribed doses or minimizing the weighted sum of the average dose on critical structures). On the other hand, Akartunalı et al. (2015) only relax the partial volume constraints of target volumes (TVs) and try to satisfy them in the objective function. Other treatment related requirements are embedded into their MILP model as hard constraints. Dursun et al. (2019*a*,*b*) apply Benders decomposition and branch-and-price to improve solution performance of a MILP model for VMAT, respectively. For more detail about rotational therapy planning we refer to the studies of Unkelbach et al. (2015), which reviews mathematical optimization methods used in VMAT planning, and Cedric & Tang (2011), which reviews mainly IMAT studies from a clinical point of view. Also, there is a recent comprehensive review of Breedveld et al. (2018) that describes the use of multi-criteria optimization and decision-making methods in radiation therapy as well as clinical details of treatment. All of these studies consider co-planar treatment. However, there are also studies that optimize VMAT plans for non-coplanar geometries obtained by couch rotation (Smyth et al. 2013, Lyu et al. 2018).

We consider a MILP model that optimizes simultaneously aperture shapes and radiation

intensities at control points. Our VMAT planning model, which we call VMATP, is based on our previous works (Dursun et al. 2016, 2019*a*,*b*). It includes CVaR constraints for partial-volume restrictions of all structures, and all treatment dose prescriptions are satisfied by the constraints as a result. The objective of VMATP is to minimize total radiation delivered to the patient. Our model, which essentially seeks an optimal VMAT plan with minimum MUs, is capable of handling many aspects of the complex decision process behind VMAT planning. However, this makes it computationally very difficult to solve exactly in order to generate optimal plans for realistic clinical cases with many OARs. In this study, we address this issue and propose an efficient two-phase heuristic that expands some algorithmic ideas that we employed in our previous work (Dursun et al. 2019*b*) for the development of a branch-and-price exact solution algorithm. In the first phase, we generate an initial full treatment arc using a two-step approach and calibrate the right hand side values of the CVaR constraints, simultaneously. We consider the rows of a full treatment arc as variables, and generate them by solving the subproblems, which are formulated as shortest path problems and solved efficiently by dynamic programming (Bellman 1952). In the second phase, we improve the initial treatment plan obtained in the first phase using column generation. Main contributions of our study can be listed as follows:

- We propose a fully automated VMAT planning algorithm that is capable of finding good plans in one run. This is in contrast with commonly used software systems, which often require multiple iterations of modifications in parameters and re-run.
- By minimizing total radiation (MUs) delivered to the patient in the objective function, it not only finds an acceptable VMAT plan that meets dose-volume restrictions, but also reduces the risk of secondary malignancy that may arise due to high integral body dose.
- Use of CVaR constraints is not widespread in VMAT planning due to their conservatism. In this study we propose a simple approach to tune the parameters of these constraints in order to make them usable without degrading quality of the resulting plans.
- Finally, we test our algorithm on nine real prostate cases. The results show that our algorithm is able to find high-quality plans for clinical size problems in reasonable times. Moreover, we consider 2 planning TVs (PTVs) and 5 OARs and make a comprehensive dose distribution evaluation for them.

The remainder of the paper is organized as follows. In Section 2 we explain our mathematical formulation. Section 3 includes the basic components of our VMAT treatment planning algorithm including *fluence map optimization* (FMO), CVaR parameter tuning, leaf sequencing, pricing problem formulation, and other necessary derivations for the column generation method. In Section 4, we provide the computational experiments and clinical comparisons on real prostate cases. Finally, Section 5 concludes the paper.

2. Mathematical model

In this section, we briefly explain our proposed mixed integer linear programming (MILP) model for the sake of completeness. Its previous versions are given in our earlier studies in detail (Dursun et al. 2016, 2019*a*). We start by discretizing some continuous parts of the VMAT planning problem.

The gantry of the linear accelerator rotates around the patient and delivers radiation continuously. We first discretize a complete tour (i.e. a full treatment arc, a 360° tour) by assuming that radiation delivery occurs at only a number of control points. This is a reasonable assumption when total number of control points (K) is large enough. At each control point radiation is delivered through the aperture formed by the multileaf collimator (MLC) mounted on the linear accelerator. A two-dimensional $m \times n$ binary matrix represents an aperture for an MLC consisting of m leaf pairs. Each row of the matrix corresponds to a leaf pair and is decomposed into n columns. The resulting mn entries of the matrix are called beamlets (bixels). Two nonnegative integer variables l_{ik} and r_{ik} represent positions of the left and right leaves, respectively, on row i ($i = 1, \ldots, m$) at control point k ($k = 1, \ldots, K$). l_{ik} is the rightmost beamlet closed by the left leaf ($0 \leq l_{ik} \leq n$). Similarly, r_{ik} is the leftmost beamlet closed by the right leaf ($1 \leq r_{ik} \leq n+1$). Note that 0 and $n+1$ are the home positions of the left and right leaves. To represent jth beamlet ($j = 1, \ldots, n$) of row i at control point k we introduce the binary variable z_{ijk}, which takes value 1 if the corresponding beamlet is open, 0 otherwise. We only consider the *consecutive ones property* of MLC systems that requires open beamlets to be consecutive. We refer the reader to the study of Gören & Taşkın (2015) for details of other possible properties of various MLC systems.

We assume that the gantry rotates around the patient at a constant speed, which may result in plans having longer treatment time than necessary. We note that Peng et al. (2015) also makes the same assumption; however, unlike our approach they also assume that dose rate is constant during the rotation. The leaves of MLC can move in order to change the shape of the beam during the rotation of the gantry. The maximum allowable distance parameter δ that a leaf can move between two adjacent control points depends on the speed of the gantry, and it is calculated in terms of beamlets. We introduce a nonnegative continuous variable mu_k for the radiation dose intensity (MU) at control point k. Dose rate (MU/second) may change during the rotation but it is constant at a control point. Also, we assume that the irradiation takes the same amount of time (tour completion time/K seconds) at each one of the control points. This indicates an upper limit on the radiation dose intensity, parameter U^{mu}, at any control point. We define another parameter, L^{mu}, which represents the lower limit on the radiation dose intensity. We also introduce a nonnegative continuous variable a_{ijk} that represents the radiation dose intensity of the jth beamlet of row i at control point k.

The body of a patient consists of different type of structures: target volumes (TVs) and organs at risks (OARs). These volumes are discretized into a number of small cubes called *voxels*. Let V_t^{TV} be the set of all voxels in TV t for $t = 1, \ldots, T$, and let V_o^{OAR} be the set of all voxels in OAR o for $o = 1, \ldots, O$. Finally, V is the set of all voxels (i.e. $V = (\cup_{t=1}^{T} V_t^{TV}) \cup (\cup_{o=1}^{O} V_o^{OAR})$). The model calculates d_v, which is a nonnegative continuous variable and indicates the amount of radiation absorbed by voxel v (in Gray, Gy). In VMAT treatment there may be two types of prescription doses for a structure. These prescriptions are satisfied by the full-volume and partial-volume constraints. There may be both types of constraints for a TV. A full-volume constraint requires that the entire volume should absorb radiation above (or below) a certain amount of radiation. L_t^{TV} and U_t^{TV} parameters are the corresponding lower and upper bounds, respectively, on the amount of radiation dose absorbed by voxels in TV t. According to a partial-volume constraint defined for TV t, at least a certain ratio α_{tc}^{TV} of its volume must absorb radiation no

less than the prescribed dose $\overline{d}_{tc}$. Note that there may be more than one partial-volume constraint defined for TV t. Thus, α_{tc}^{TV} and $\overline{d}_{tc}$ parameters demonstrate the ratio and the prescribed dose of the cth partial-volume constraint of TV t, respectively, for $c = 1, \ldots, C_t$. On the other hand, a partial-volume constraint defined for OAR o requires that the ratio of the volume absorbing radiation at most tolerance dose U_{oc} must be at least α_{oc}^{OAR}. Similarly, α_{oc}^{OAR} and U_{oc} parameters represent the corresponding ratio and the tolerance dose of the cth partial-volume constraint of OAR o for $c = 1, \ldots, C_o$. The mixed integer linear programming model for VMAT planning, which we call VMATP, then reads:

VMATP:

$$\min \sum_{k=1}^{K} mu_k \tag{1}$$

$s.t.$

$$r_{ik} - jz_{ijk} \geq 1 \qquad i = 1,\ldots,m;\ j = 1,\ldots,n;\ k = 1,\ldots,K \tag{2}$$

$$(n+1-j)z_{ijk} + l_{ik} \leq n \qquad i = 1,\ldots,m;\ j = 1,\ldots,n;\ k = 1,\ldots,K \tag{3}$$

$$r_{ik} - l_{ik} - \sum_{j=1}^{n} z_{ijk} = 1 \qquad i = 1,\ldots,m;\ k = 1,\ldots,K \tag{4}$$

$$l_{i(k+1)} - l_{ik} \leq \delta \qquad i = 1,\ldots,m;\ k = 1,\ldots,K-1 \tag{5}$$

$$l_{ik} - l_{i(k+1)} \leq \delta \qquad i = 1,\ldots,m;\ k = 1,\ldots,K-1 \tag{6}$$

$$r_{i(k+1)} - r_{ik} \leq \delta \qquad i = 1,\ldots,m;\ k = 1,\ldots,K-1 \tag{7}$$

$$r_{ik} - r_{i(k+1)} \leq \delta \qquad i = 1,\ldots,m;\ k = 1,\ldots,K-1 \tag{8}$$

$$a_{ijk} \leq U^{mu} z_{ijk} \qquad i = 1,\ldots,m;\ j = 1,\ldots,n;\ k = 1,\ldots,K \tag{9}$$

$$a_{ijk} \geq mu_k - U^{mu}(1 - z_{ijk}) \qquad i = 1,\ldots,m;\ j = 1,\ldots,n;\ k = 1,\ldots,K \tag{10}$$

$$a_{ijk} \leq mu_k \qquad i = 1,\ldots,m;\ j = 1,\ldots,n;\ k = 1,\ldots,K \tag{11}$$

$$d_v - \sum_{i=1}^{m}\sum_{j=1}^{n}\sum_{k=1}^{K} D_{ijkv} a_{ijk} = 0 \qquad v \in V \tag{12}$$

$$\xi_{tc}^{TV} - \frac{1}{(1-\alpha_{tc}^{TV})|V_t^{TV}|} \sum_{v \in V_t^{TV}} x_{tcv} \geq \overline{d}_{tc} \qquad t = 1,\ldots,T;\ c = 1,\ldots,C_t \tag{13}$$

$$x_{tcv} \geq \xi_{tc}^{TV} - d_v \qquad t = 1,\ldots,T;\ c = 1,\ldots,C_t;\ v \in V_t^{TV} \tag{14}$$

$$\xi_{oc}^{OAR} + \frac{1}{(1-\alpha_{oc}^{OAR})|V_o^{OAR}|} \sum_{v \in V_o^{OAR}} y_{ocv} \leq U_{oc} \qquad o = 1,\ldots,O;\ c = 1,\ldots,C_o \tag{15}$$

$$y_{ocv} \geq d_v - \xi_{oc}^{OAR} \qquad o = 1,\ldots,O;\ c = 1,\ldots,C_o;\ v \in V_o^{OAR} \tag{16}$$

$$d_v \geq L_t^{TV} \qquad t = 1,\ldots,T;\ v \in V_t^{TV} \tag{17}$$

$$d_v \leq U_t^{TV} \qquad t = 1,\ldots,T;\ v \in V_t^{TV} \tag{18}$$

$$mu_k \geq L^{mu} \qquad k = 1,\ldots,K \tag{19}$$

$$mu_k \leq U^{mu} \qquad k = 1,\ldots,K \tag{20}$$

$$\mathbf{l} \in \mathbb{Z}_+^{m\times K};\ \mathbf{r} \in \mathbb{Z}_+^{m\times K};\ \mathbf{z} \in \{0,1\}^{m\times n\times K} \tag{21}$$

$$\mathbf{mu} \in \mathbb{R}_+^K;\ \ \mathbf{a} \in \mathbb{R}_+^{m\times n\times K} \tag{22}$$

$$\mathbf{d} \in \mathbb{R}_+^{|V|};\ \ \mathbf{x} \in \mathbb{R}_+^{\sum_{t=1}^{T} C_t|V_t^{TV}|};\ \ \mathbf{y} \in \mathbb{R}_+^{\sum_{o=1}^{O} C_o|V_o^{OAR}|} \tag{23}$$

$$\xi^{\mathbf{TV}} \in \mathbb{R}^{\sum_{t=1}^{T} C_t};\ \ \xi^{\mathbf{OAR}} \in \mathbb{R}^{\sum_{o=1}^{O} C_o}. \tag{24}$$

Constraints (2)–(4) ensure the consecutive ones property of the binary matrices representing the apertures. They ensure that left and right leaves in each row do not overlap. Also, they guarantee that z_{ijk} variables, associated with only open beamlets (i.e. the beamlets between the leaf pairs), are 1. Movement of the leaves during rotation is controlled by constraints (5)–(8). Radiation passes through only the open beamlets, and constraints (9)–(11) ensure that a_{ijk} variable equals to mu_k if associated beamlet is open, and 0 otherwise. Constraint (12) calculates the radiation dose absorbed by voxel v. Note that $\mathbf{D}$ is the dose-influence matrix, where D_{ijkv} specifies the dose contribution (in Gy/MU) to voxel v from beamlet (i, j) at control point k. Constraints (9)–(12) are equivalent to the linearization of

$$d_v = \sum_{i=1}^{m}\sum_{j=1}^{n}\sum_{k=1}^{K} D_{ijkv} z_{ijk} mu_k \qquad\qquad v \in V \tag{25}$$

by means of McCormick's envelope (McCormick 1976). The right hand side expression of (25) includes the product of binary variables $\mathbf{z}$ with the continuous variables $\mathbf{mu}$, thus it is nonlinear. We formulate the dose-volume constraints (13)–(16) for each TV and OAR as conditional value-at-risk (CVaR) constraints similar to the studies of Romeijn et al. (2003, 2006) and Gozbasi (2010). The CVaR approach was originally developed by Rockafellar et al. (2000) for portfolio optimization. Constraints (13)–(14) ensure that the *lower mean tail dose at level* α_{tc}^{TV}, namely the average radiation dose of (1-α_{tc}^{TV})$|V_t^{TV}|$ voxels in TV t absorbing the lowest radiation, is at least $\overline{d}_{tc}$. Similarly, constraints (15)–(16) ensure that the *upper mean tail dose at level* α_{oc}^{OAR}, namely the average dose of (1-α_{oc}^{OAR})$|V_o^{OAR}|$ voxels absorbing the highest radiation, is at most U_{oc}. As discussed in Romeijn et al. (2003), continuous variable ξ_{oc}^{OAR} in constraint (15) is a bound on the upper value-at-risk (VaR) at level α_{oc}^{OAR}, which is the smallest dose level with the property that no more than $100(1-\alpha_{oc}^{OAR})\%$ of OAR o receives a larger dose. Furthermore, the left hand side of constraint (15) is the upper α_{oc}^{OAR}-CVaR, which is the mean of all doses that exceed the upper α_{oc}^{OAR}-VaR. The variable y_{ocv} is the surplus of the value ξ_{oc}^{OAR} by the dose received by voxel v in OAR o. Note that if constraint (15) is satisfied as an equality in an optimal solution, then ξ_{oc}^{OAR} equals to the VaR corresponding to that constraint. Also note that the number of constraints (14) and (16) depends on the number of voxels and the number of partial-volume constraints; they are respectively $\sum_{t=1}^{T} C_t|V_t^{TV}|$ and $\sum_{o=1}^{O} C_o|V_o^{OAR}|$. Similarly, the number of constraints (13) and (15) are equal to total number of partial-volume constraints defined for target volumes ($\sum_{t=1}^{T} C_t$) and OARs ($\sum_{o=1}^{O} C_o$), respectively. Constraints (17)–(18) are full-volume constraints defined for TV t. Constraints (19)–(20) limit the radiation intensity at each one of the control points. Equations (21)–(24) define the variables. Finally, (1) is the objective function that minimizes total radiation intensity delivered to the patient during treatment.

3. Proposed method

VMATP determines K sequential apertures (a *full treatment arc*) satisfying all geometry constraints of MLC system. It also finds the radiation intensity of each one of the control points. We first observe that if we are given the full treatment arc, then the problem reduces to finding the radiation intensities only. Using this observation we decompose VMATP into two subproblems. We also note that the apertures are interdependent because of the leaf motion limitations. However, we only consider the consecutive ones property and the rows of a treatment arc are independent. This makes it possible to decompose a full treatment arc into m rows that satisfy the leaf motion limitations and the consecutive ones property, which we refer to as *row arcs*. We note that such a decomposition is not possible in the presence of interdigitation constraints. Let $Z_i = \{\mathbf{z}_i^1, \mathbf{z}_i^2, \ldots, \mathbf{z}_i^e, \ldots, \mathbf{z}_i^{|Z_i|}\}$ be the set of all feasible row arcs of row i, where $\mathbf{z}_i^e = \{\hat{z}_{ijk}^e \in \{0,1\},\ \ j = 1, \ldots, n; k = 1, \ldots, K\}$. Let also Z_i^0 be a subset of Z_i. We introduce b_i^e binary variable to the master problem (MP) that are set to 1 if the corresponding feasible row arc $\mathbf{z}_i^e$ is selected, 0 otherwise. We solve the linear programming relaxation of MP with the subset Z_i^0 for each row i. Moreover, we introduce one nonnegative artificial variable (ϕ_{tc}^{TV} or ϕ_{oc}^{OAR}) for each one of the CVaR constraints (13 and 15) to allow deviations. We penalize positive deviations in the objective function. Then the resulting modified restricted linear master problem (M-RLMP) becomes

M-RLMP:

$$\min \sum_{k=1}^{K} mu_k + \sum_{t=1}^{T}\sum_{c=1}^{C_t} \gamma_{tc}^{TV}\phi_{tc}^{TV} + \sum_{o=1}^{O}\sum_{c=1}^{C_o} \gamma_{oc}^{OAR}\phi_{oc}^{OAR} \tag{26}$$

s.t.

$$(11)-(12);\ \ (14);\ \ (16)-(20);\ \ (22)-(24),$$

$$\sum_{e=1}^{|Z_i^0|} b_i^e = 1 \qquad i = 1, \ldots, m \tag{27}$$

$$-a_{ijk} + U^{mu} \sum_{e=1}^{|Z_i^0|} b_i^e \hat{z}_{ijk}^e \geq 0 \qquad i = 1, \ldots, m; j = 1, \ldots, n; k = 1, \ldots, K \tag{28}$$

$$a_{ijk} - mu_k - U^{mu} \sum_{e=1}^{|Z_i^0|} b_i^e \hat{z}_{ijk}^e \geq -U^{mu} \qquad i = 1, \ldots, m; j = 1, \ldots, n; k = 1, \ldots, K \tag{29}$$

$$\xi_{tc}^{TV} - \frac{1}{(1-\alpha_{tc}^{TV})|V_t^{TV}|} \sum_{v \in V_t^{TV}} x_{tcv} + \phi_{tc}^{TV} \geq \overline{d}_{tc} \qquad t = 1, \ldots, T; c = 1, \ldots, C_t \tag{30}$$

$$\xi_{oc}^{OAR} + \frac{1}{(1-\alpha_{oc}^{OAR})|V_o^{OAR}|} \sum_{v \in V_o^{OAR}} y_{ocv} - \phi_{oc}^{OAR} \leq U_{oc} \quad o = 1, \ldots, O; c = 1, \ldots, C_o \tag{31}$$

$$\mathbf{b} \in \mathbb{R}_+^{\sum_{i=1}^{m} |Z_i^0|};\ \ \phi^{\mathbf{TV}} \in \mathbb{R}_+^{\sum_{t=1}^{T} C_t} \tag{32}$$

$$\phi^{\mathbf{OAR}} \in \mathbb{R}_+^{\sum_{o=1}^{O} C_o}. \tag{33}$$

Here γ_{tc}^{TV} and γ_{oc}^{OAR} are large penalty costs for deviations in the cth partial-volume constraints of

TVs t and OAR o, respectively. Also, $\hat{z}^e_{ijk}$ becomes a parameter in this model, which takes on value 1 or 0 and indicates whether the jth beamlet of row i at control point k is open or not, respectively. Note that if the leaf motion limitations are not considered then the size of Z_i for each row is $\left(\frac{1}{2}(n+1)(n+2)\right)^K$, hence total number of feasible treatment row arcs is $m\left(\frac{1}{2}(n+1)(n+2)\right)^K$. Thus, solving linear programming relaxation of MP including all columns is not tractable. Instead, we iteratively solve M-RLMP and search for new promising row arcs (columns for M-RLMP) by solving m pricing subproblems (PSPs). Then, we replace the current columns with the newly generated ones having negative reduced cost while ensuring that each row arc has a corresponding column in the formulation. We discuss the details of our column generation approach in the following sections.

3.1. Pricing subproblem

Let $\hat{\lambda}_i$, $\hat{\beta}^1_{ijk}$ and $\hat{\beta}^2_{ijk}$ be the optimal dual values associating with constraints (27)–(29). In column generation iterations, for each row i the following subproblem PSP_i is solved to optimality to find a row arc with minimum reduced cost. If the resulting reduced cost is negative then the corresponding row arc is added to the M-RLMP. On the other hand, if there is no row arc with negative reduced cost for any row i then we are at an optimal solution of M-RLMP.

PSP_i:

$$\min -\hat{\lambda}_i - U^{mu}\sum_{k=1}^{K}\sum_{j=1}^{n}(\hat{\beta}^1_{ijk}-\hat{\beta}^2_{ijk})z_{ijk} \tag{34}$$

s.t.

$$r_{ik} - jz_{ijk} \geq 1 \qquad j=1,\ldots,n;\ \ k=1,\ldots,K \tag{35}$$

$$(n+1-j)z_{ijk} + l_{ik} \leq n \qquad j=1,\ldots,n;\ \ k=1,\ldots,K \tag{36}$$

$$r_{ik} - l_{ik} - \sum_{j=1}^{n} z_{ijk} = 1 \qquad k=1,\ldots,K \tag{37}$$

$$l_{i(k+1)} - l_{ik} \leq \delta \qquad k=1,\ldots,K-1 \tag{38}$$

$$l_{ik} - l_{i(k+1)} \leq \delta \qquad k=1,\ldots,K-1 \tag{39}$$

$$r_{i(k+1)} - r_{ik} \leq \delta \qquad k=1,\ldots,K-1 \tag{40}$$

$$r_{ik} - r_{i(k+1)} \leq \delta \qquad k=1,\ldots,K-1 \tag{41}$$

$$\mathbf{l} \in \mathbb{Z}^K_+;\ \ \mathbf{r} \in \mathbb{Z}^K_+;\ \ \mathbf{z} \in \{0,1\}^{n\times K}. \tag{42}$$

At optimality of M-RLMP, if all b^e_i variables are integer then we have also an optimal solution for VMATP. However, this is a rare situation and generally optimal values of b^e_i variables are fractional, which does not provide a feasible VMAT treatment plan. In order to resolve this problem, we start with only one row arc for each one of the rows in our heuristic approach. Namely, there is only one column for each row arc i in the initial column pool. Hence, there is only one b^1_i variable that takes value of 1 at optimality. Therefore, the optimal solution yields a full treatment arc that is feasible in terms of geometry constraints of MLC. Each time a new promising row arc is generated we replace the current one with this new arc to ensure that there

remains exactly one column for each row i in the column pool (i.e. the size of the column pool for each row $|Z_i^0| = 1$).

We note that replacing an existing column with a new one may worsen the objective function value. The reason is that the new column is not guaranteed to improve the objective function value in the absence of the existing set of columns. We employ a specialized column generation strategy to ensure that the objective function value does not worsen in subsequent iterations of our algorithm. We first observe that often a subset of control points has positive radiation intensity (i.e. $mu_k > 0$) in an optimal solution of M-RLMP, whereas radiation intensity values associated with the remaining control points are zero. Based on this observation, our column generation strategy ensures that leaf positions corresponding to control points having $mu_k > 0$ are kept constant between successive iterations. This strategy ensures that the previous solution stays feasible with respect to the new set of columns, and therefore the objective function value does not deteriorate in successive iterations.

Network models have been applied in radiation therapy planning studies to solve the MLC sequencing problem in IMRT planning (Boland et al. 2004) and to generate a treatment arc in VMAT planning (Gozbasi 2010, Mahnam et al. 2017). We use a network structure similar to the one in Gozbasi (2010) and formulate our pricing problem as a shortest path problem. The layers represent the control points and at each layer there are $\frac{(n+1)(n+2)}{2}$ nodes stand for the possible leaf configurations satisfying the consecutive ones property. There are additional two layers including a dummy start and finish node. There is an arc between two nodes at two consecutive control points if they are compatible, namely the leaf motion limitations are satisfied. Note that the arcs of the network are directed, since we assume the gantry rotates in one direction. Furthermore, there is no arc between any two nodes at the same control point. Thus, the network is acyclic. We solve this problem using dynamic programming. If we do not consider leaf motion limitations, then there are $\frac{(K-1)}{4}(n+1)^2(n+2)^2 + (n+1)(n+2)$ arcs in the network. Thus, solving by dynamic programming takes $O(Kn^4)$ time in the worst case, which makes it a polynomial time procedure. Finally, the cost of arcs are derived using the dual optimal solution of M-RLMP. Hence, $-U^{mu}\sum_{j=l+1}^{j=r-1}(\hat{\beta}_{ijk}^1 - \hat{\beta}_{ijk}^2)$ is the cost of an arc that connects two nodes from control points k and $k+1$ (i.e. the arc only carries the cost of the node at control point k). Thus, there is no cost on an arc between the start node and the nodes at the first control point. Let C be the cost of a shortest path in the network, then the minimum reduced cost is $C - \hat{\lambda}_i$.

Figure 1 illustrates a small network of PSP with 2 control points ($K = 2$) and 2 columns ($n = 2$). Also, the maximum distance that a leaf can take between two stages is 1 beamlet ($\delta = 1$). There are 6 different leaf configurations at each one of the stages. The white and gray rectangles indicate the open and closed beamlets, respectively. The home positions of the left and right leaves are $j = 0$ and $j = 3$ and capital letters "L" and "R" shows the last blocked beamlets by the left and right leaves, respectively. The arcs indicate the feasible leaf movements. Let the path in the figure with solid lines indicate a shortest path. Then, the positions of the leaf pair during rotation are $(l_{i1} = 0, r_{i1} = 2)$ and $(l_{i2} = 1, r_{i2} = 3)$.

Finally, each time when we solve PSP for row i, we fix the leaf positions at the control points having positive radiation intensity in the last optimal M-RLMP solution. Let k be such a control point with positive radiation intensity (i.e. $mu_k > 0$). We remove all other nodes that are different

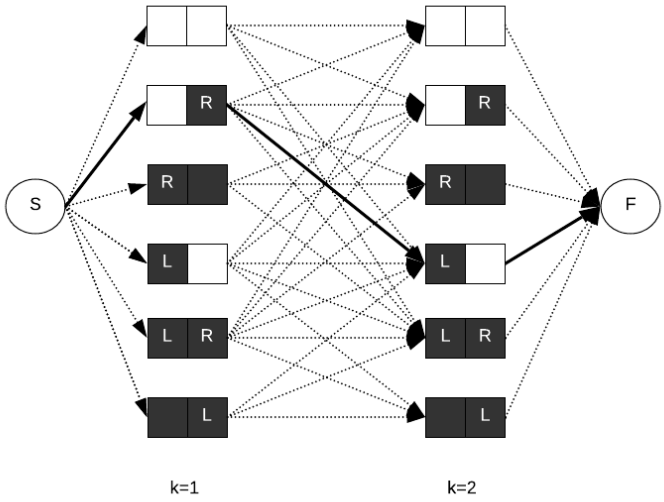

Figure 1. Network representation of a PSP where $K = 2$, $n = 2$, $\delta = 1$.

from the leaf configuration of the last optimal M-RLMP solution on row i at control point k.

Remark 1: When the size of the column pool for each row i is one, the associated variable b_i^1 takes value 1 for any optimal solution to the M-RLMP. In this case, certain simplifications can be made to our proposed column generation approach. In particular, the simplified versions of the constraints (28) and (29) become $-a_{ijk} + U^{mu}\hat{z}_{ijk}^1 \geq 0$ and $a_{ijk} - mu_k - U^{mu}\hat{z}_{ijk}^1 \geq -U^{mu}$, respectively. Furthermore, for these constraints the corresponding dual variables (β_{ijk}^1 and β_{ijk}^2) remain the same, and this simplification reveals the role of dual values more clearly. In the first case, when a particular beamlet is closed ($\hat{z}_{ijk}^1 = 0$), its constraint (28) becomes $a_{ijk} \leq 0$, namely the corresponding beamlet intensity is zero. If this constraint limits the optimal value of M-RLMP and its corresponding dual value β_{ijk}^1 is positive, then PSP will try to open that particular beamlet in order to reduce the cost (i.e. z_{ijk} will be 1 and the constraint (28) will be $a_{ijk} \leq U^{mu}$). In the second case, if a particular beamlet is open ($z_{ijk} = 1$) then the beamlet intensity takes value mu_k. Similarly, if this constraint limits the optimal value of M-RLMP and dual value β_{ijk}^2 is positive, then closing this particular beamlet will reduce the cost. Therefore, PSP will close that beamlet ($z_{ijk} = 0$) and the constraint (29) will become $a_{ijk} \geq mu_k - U^{mu}$.

Remark 2: When the size of the column pool for each row i is one, main role of M-RLMP becomes finding the optimum radiation intensity, mu_k, for a subset of given apertures and calculating corresponding dual multipliers. Moreover, PSP finds the best promising row arc for each row i, and it adjusts apertures.

3.2. Initial column generation

At the beginning there is exactly one column (one row arc) for each row i in the initial column pool to formulate M-RLMP. Their union yields a full treatment arc consisting of K apertures

(one aperture per control point). We apply a simple heuristic consisting of two steps to generate these initial columns. At the first step a number of fluence maps are generated by solving a linear programming model, and in the second step using a simple fluence map conversion algorithm a full treatment arc, which yields a column per each row, is constructed. Finally, M-RLMP is formulated. Note that dose intensities of all control points are determined by M-RLMP, namely mu_k is a decision variable for control point k to be optimized. These steps constitute the first phase of our two-phase algorithm. In the second phase, this initial full arc is modified during the column generation iterations in order to obtain a better treatment plan, so it is very important to start with good columns.

3.2.1. Fluence map generation: The linear programming (LP) model that we solve in the first step is derived from VMATP and includes only a subset of original control points and constraints. Note that, as in this study, K is generally taken 180 in VMAT planning studies (i.e. 180 equally spaced beam angles with 2°-spacing). The LP model, namely the modified VMATP (M-VMATP) includes 45 control points with 8°-spacing. We let $\overline{K}$ denote this subset of control points. Similar to M-RLMP, we introduce one artificial variable for each CVaR constraint of all OARs to M-VMATP, and penalize the positive deviations in the objective function. We allow these deviations not only because M-VMATP includes only a subset of control points but also because at the beginning CVaR constraints consisting of the original tolerance doses are very tight. Thus, finding a treatment plan which satisfies all treatment dose prescriptions is very hard. The M-VMATP is as follows:

M-VMATP:

$$\min \sum_{k\in\overline{K}} mu_k + \sum_{o=1}^{O}\sum_{c=1}^{C_o} \gamma_{oc}^{OAR}\phi_{oc}^{OAR} \tag{43}$$

s.t.

$$(13)-(14);\ \ (16)-(18);\ \ (23)-(24);\ \ (31);\ \ (33),$$

$$a_{ijk} \le mu_k \qquad i=1,\dots,m;\ \ j=1,\dots,n;\ \ k\in\overline{K} \tag{44}$$

$$d_v - \sum_{i=1}^{m}\sum_{j=1}^{n}\sum_{k\in\overline{K}} D_{ijkv}a_{ijk} = 0 \qquad v\in V \tag{45}$$

$$mu_k \ge L^{mu} \qquad k\in\overline{K} \tag{46}$$

$$mu_k \le U^{mu} \qquad k\in\overline{K} \tag{47}$$

$$\mathbf{mu}\in\mathbb{R}_+^{|\overline{K}|};\ \ \mathbf{a}\in\mathbb{R}_+^{m\times n\times|\overline{K}|}. \tag{48}$$

Solving this modified model has similarities with FMO optimization in IMRT planning. M-VMATP finds a number of fluence maps for some of the control points in $\overline{K}$, which we denote as $\overline{\overline{K}}$. Notice that $\overline{\overline{K}} \subset \overline{K} \subset K$. However, $\overline{\overline{K}}$, the set of control points with positive intensities, is not determined in advance; M-VMATP model finds it. Also, the intensities of the beamlets of a fluence map are bounded from above with radiation intensity at this control point (mu_k). Observe that if there is no beamlet with positive intensity at control point k then mu_k value will be 0, since total radiation intensity is minimized in the objective function. Furthermore, in this step, in addition to

generating fluence maps we also tune the parameters U_{oc} of CVaR constraints of OARs to obtain more reasonable feasible treatment plans. In a loop, we increase the tolerance dose U_{oc} by a small value if the difference between the radiation dose that the corresponding volume of OAR o receives and the original tolerance dose is at least a certain amount, and resolve M-VMATP model until there remains no parameter to increase. At the end of this loop, if there is a CVaR constraint with positive deviation we increase its right hand side parameter by the amount of deviation. We use the resulting tuned parameters throughout the entire algorithm.

3.2.2. Tuning of CVaR constraints: The main advantage of using CVaR constraints is that it allows modeling of dose volume requirements as linear inequalities. However, we observe that CVaR constraints with original parameters are very conservative and it is challenging to apply this approach in radiation therapy planning, which is also indicated in Romeijn et al. (2003) and Hindi (2013). Let us consider a CVaR constraint defined for an OAR. It forces the average dose in the upper tail of the dose distribution of the OAR to be at most its tolerance dose. However, the fact that the left end of the tail (i.e. VaR) does not exceed this tolerance dose is sufficient in a clinically acceptable plan (Hindi 2013). In order to alleviate this problem we tune the right hand side values, i.e. U_{oc} of the CVaR constraints of OARs. We change these parameters in such a way that the resulting ones continue to produce treatment plans satisfying clinical prescription doses. In particular, we solve M-VMATP and check whether the VaR values are too small than the corresponding bounds; if they are, we update the right hand sides of the constraints. In each iteration we do this operation for all OARs, after that we resolve M-VMATP. We continue until there remains no CVaR constraint that we can update. The pseudo code of this parameter tuning procedure is given below. Note that it is not appropriate to use the same right hand side values for all patients due to the anatomical differences between them. Thus, it is convenient to use such an adaptive procedure for tuning the right hand side values for each patient.

3.2.3. Conversion algorithm: In the second step we derive a number of apertures (at most three) from each one of the fluence maps obtained in the first step using a conversion algorithm. Clearly, in a fluence map, the beamlets with positive radiation intensity do not have to satisfy the consecutive ones property, also their intensities may differ from each other. We assume that all beamlets with positive intensity are open. Our conversion algorithm seeks at most three feasible apertures to cover the open beamlets as much as possible. If all open beamlets of all rows are consecutive in a fluence map at control point k, then we generate only one aperture and fix it at k. If there are at most two open beamlet chains at each row than we generate two different apertures and sequence them on to control points k and $k+2$. Otherwise, if there are rows with more than two open beamlet chains than we generate three different apertures and sequence them on to control points on to k, $k+1$, and $k+2$. There are two important details in the generation of these apertures. First, an aperture must be compatible with the fixed ones at the adjacent control points. Namely, the leaf motion limitations must be satisfied. If a row of an aperture is not compatible with the adjacent ones we close all beamlets in this row. The second point is that we first fix the aperture at k, and then $k+2$. If there is a third aperture, finally we fix it at $k+1$. After sequencing all apertures on to a subset of K, we fill the missing control points in such a way that the number of

Algorithm CVaR parameter tuning

ϵ_1, ϵ_2, counter $= 0$
while true **do**
  update and solve M-VMATP
  for each o in OARs and c in C_o **do**
    if $\xi_{oc}^{OAR} < U_{oc} - \epsilon_1$ **then**
      $U_{oc} \leftarrow U_{oc} + \epsilon_2$
      counter $\leftarrow$ counter+1
    end if
  end for
  if counter $= 0$ **then**
    break
  else
    counter $= 0$
  end if
end while
for each o in OARs and c in C_o **do**
  if $\phi_{oc}^{OAR} > 0$ **then**
    $U_{oc} \leftarrow U_{oc} + \phi_{oc}^{OAR}$
  end if
end for

open beamlets in the resulting arc is maximum. Namely, we open all the beamlets as long as they are compatible with the ones at fixed apertures. Thus, we obtain a full treatment arc (consisting of K sequential apertures) to construct M-RLMP. The pseudo code of this conversion algorithm is given below.

The first two rows of Figure 2 illustrate the conversion of a fluence map at the fifth control point (gantry angle 8°) into three apertures and their sequencing. The fluence map is decomposed into three apertures. The rows of the aperture at k=5 are the first consecutive beamlet chains from the left part of the fluence map. If there is more than one open beamlet chain at any row then we need another aperture to complete the fluence map. The aperture at control point 7 consists of the first open beamlet chains of the rows from the right. Finally, at control point 6, there is an aperture with one beamlet at the second row, since there are three open beamlet chains at the second row of the fluence map. Also, there is an open beamlet at third row in order to make the apertures at control points 5 and 6 compatible (i.e. satisfying leaf motion limitations). At the last row of the figure, the part of the full treatment arc between 8° and 16° is shown where $\delta = 2$.

In summary, our proposed two-phase algorithm starts by generating initial columns to construct M-RLMP in the first phase that includes two steps: solving M-VMATP to obtain a number of fluence maps, and generating a full treatment arc from these fluence maps by applying the conversion algorithm. Initially there is only one column for each row i at M-RLMP, and they are improved in column generation iterations in the second phase. The flow diagram of the resulting algorithm is given in Figure 3.

Algorithm Conversion algorithm

Input: a number of fluence maps
Output: a full treatment arc
for the fluence map at control point $k \in \overline{\overline{K}}$ **do**
    for row $i = 1, \ldots, m$ **do**
        if all beamlets with positive intensity are consecutive **then**
            generate a row with one open beamlet chain
            if it is compatible with the previous control points in K **then**
                fix it at row i at control point k
            else
                close all beamlets at row i at control point k
            end if
        else
            generate a row including the first open beamlet chain from the left
            if it is compatible with the previous control points in K **then**
                fix it at row i at control point k
            else
                close all beamlets at row i at control point k
            end if
            generate a row including the first open beamlet chain from the right
            if it is compatible with the previous control points in K **then**
                fix it at row i at control point $k + 2$
            else
                close all beamlets at row i at control point $k + 2$
            end if
        end if
    end for
end for
for fluence map at control point $k \in \overline{\overline{K}}$ **do**
    for row $i = 1, \ldots, m$ **do**
        if there are more than two positive beamlet chains **then**
            generate a row including the second open beamlet chain from the left
            if it is compatible with control points k and $k + 2$ **then**
                fix it at row i at control point $k + 1$
            end if
        end if
    end for
    if at least one row is fixed at control point $k + 1$ **then**
        find compatible apertures for control point k+1 with minimum number of open beamlets
    end if
end for
find compatible apertures with maximum number of open beamlets for the control points without any fixed rows

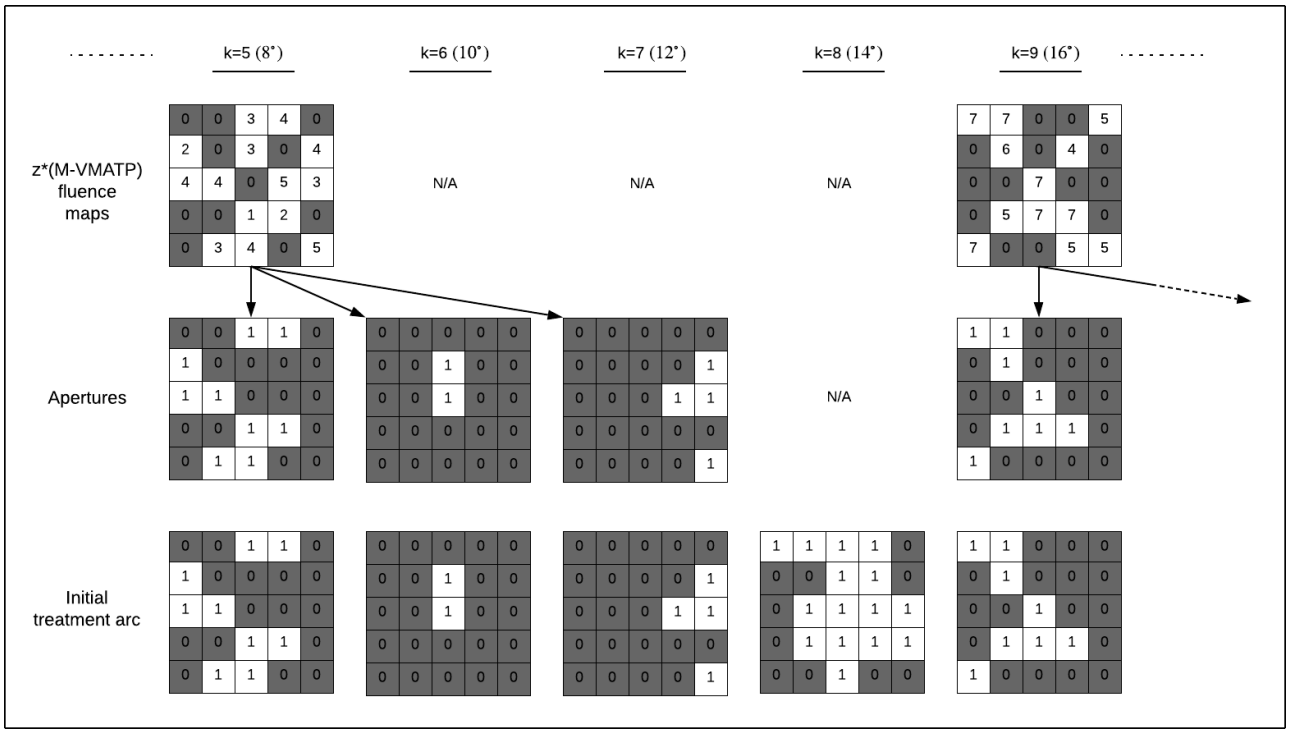

Figure 2. Initial column (initial treatment arc) generation.

4. Computational results and clinical comparisons

We generate VMAT plans for nine prostate cancer patients treated in Istanbul University Oncology Institute, which is one of the largest and oldest cancer centers in Turkey. Annually, an average of 5,000 new patients apply at the institute, and 60,000 patients are called for follow-up and control. Every day around 120-150 patients undergo radiotherapy and 90-100 patients receive chemotherapy. In our experiments, we used a number of computed tomography (CT) images with 2.5 mm spacing and a radiation therapy (RT) structure set of each one of the patients in digital imaging and communications in medicine (DICOM) format (Pianykh 2009). There are two planning target volumes (PTVs) with different prescription doses (75.6 Gy and 56 Gy in 36 fractions, respectively) and 5 OARs (rectum, bladder, penile bulb, left and right femoral heads) in each case. In radiation therapy planning there are three main volumes to be considered: gross tumor volume (GTV), clinical target volume (CTV), and PTV. The CTV contains the GTV, which is the primary tumor, and subclinical microscopic malignant lesions. The PTV surrounds the CTV and a margin to account for uncertainties in planning or delivery, and it is included in treatment planning optimization. Therefore, the terms PTV and TV are used interchangeably in the rest of the paper. Table 1 lists all structure dose constraints used for prostate radiation therapy optimization at Istanbul University Oncology Institute in accordance with the recommendation of Buyyounouski et al. (2006). There are two partial-volume constraints for each one of rectum and bladder, and for the remaining structures there is only one constraint. We use the constraints given

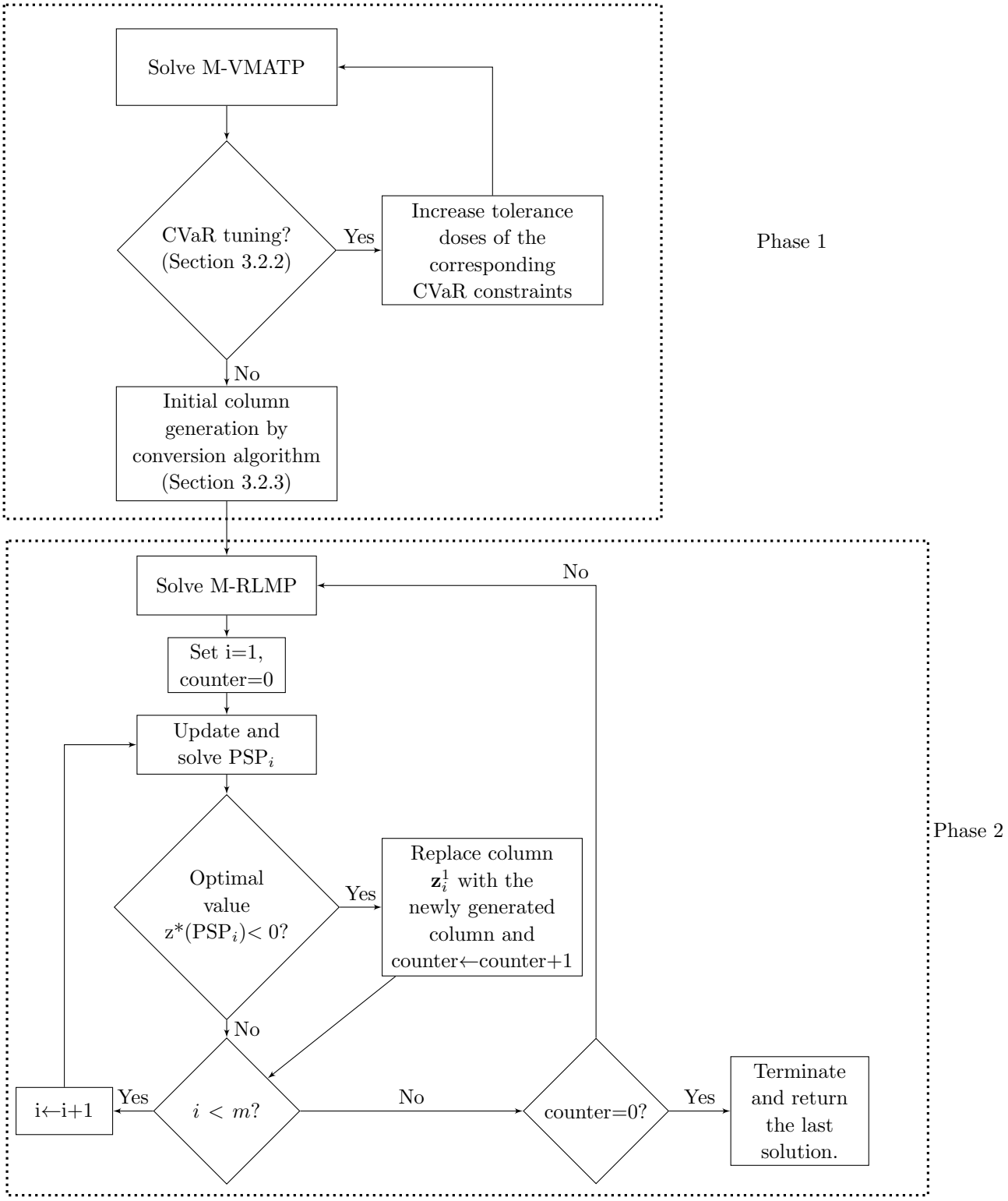

Figure 3. Flow diagram of the VMAT planning heuristic.

in Table 1 and aim to deliver 75.6 Gy in 36 fractions (2.1 Gy per fraction). Table 1 also includes the corresponding ratios of all volumes used to formulate VMATP model. Also, the value of $\overline{d}_{tc}$ and U_{oc} parameters equal to dose amounts prescribed for one fraction. In general, dose-volume histograms (DVHs) are used to evaluate the quality of a treatment plan. For a given structure, a DVH specifies the percentage of its volume that absorbs at least a certain amount of dose. We calculate DVHs of PTVs and OARs and compare them to the clinical guidelines and also to the ones obtained in the institute.

Table 1. Dose-volume constraints used at Istanbul University Oncology Institute.

Structure	$\mathbf{D_{x\%}}^*$	**Dose (in 36 fractions)**	**Ratio of volume**
PTV75.6	$D_{95\%}$	75.6 Gy	$\alpha_{11}^{PTV} = 0.95$
R-PTV56	$D_{95\%}$	56 Gy	$\alpha_{21}^{PTV} = 0.95$
Rectum	$D_{35\%}$	$\leq$ 40 Gy	$\alpha_{11}^{OAR} = 0.65$
	$D_{17\%}$	$\leq$ 65 Gy	$\alpha_{12}^{OAR} = 0.83$
Bladder	$D_{50\%}$	$\leq$ 40 Gy	$\alpha_{21}^{OAR} = 0.50$
	$D_{25\%}$	$\leq$ 65 Gy	$\alpha_{22}^{OAR} = 0.75$
PB	$D_{90\%}$	$\leq$ 15 Gy	$\alpha_{31}^{OAR} = 0.10$
Lt F	$D_{10\%}$	$\leq$ 50 Gy	$\alpha_{41}^{OAR} = 0.90$
Rt F	$D_{10\%}$	$\leq$ 50 Gy	$\alpha_{51}^{OAR} = 0.90$

$^*\mathbf{D_{x\%}}$: the minimum dose received by x% of the structure.

Istanbul University Oncology Institute currently uses Varian Eclipse Treatment Planning System (TPS) v.15.6 (Varian 2018), which is a commercial software. Thus, it is not possible to export the dose-influence matrices calculated by using Analytical Anisotropic Algorithm (AAA) algorithm (Sievinen et al. 2005). Therefore, we compute these matrices for a 6 MV photon energy using an open-source radiation TPS called matRad (Wieser et al. 2017). matRad is a multi-modality radiation TPS written in MATLAB (MATLAB 2015), and supports IMRT treatment planning for photons, scanned protons, and scanned carbon ions at clinically adequate resolution. It is freely available online and has been developed to contribute to educational and research activities. It uses a singular value decomposed pencil beam algorithm to calculate photon dose calculation (Bortfeld et al. 1993). We set the voxel resolution to 5 mm^3 and bixel resolution to 1 cm^2 during the DICOM import. The couch angle is selected as 0° for all patients and dose-influence matrices for 180 evenly spaced control points (gantry angles) with 2°-spacing are computed. Then, we scale the dose-influence matrices in such a way that the absorbed dose of 1 cGy/MU is delivered at 100 cm source-to-axis distance (SAD) at 5 cm depth with field size 10 cm $\times$ 10 cm. Thus, we divide original dose-influence matrices by the parameter 100 to obtain Gy/MU values. In other words, they are scaled such that a weight of 1 is equivalent to 100 MU. We also validate this scaling parameter on a water equivalent phantom provided by Istanbul University Oncology Institute. We list total number of voxels in each structure of all patients in Table 2. Note that, matRad's dose calculation is restricted to the projection of the target onto the beam's eye view (BEV) at each control point. Thus, for each case, we determine the smallest MLC system

size (i.e. value of m and n, in Table 2) that includes all beamlets in the matrices provided by matRad. Furthermore, a TV t may invade an OAR o, namely there may be a set of voxels in an OAR o which also belong to a TV. In such a case the overlap region is considered to belong to the TV t and the CVaR constraint is reformulated for the rest of OAR o. However, the entire OAR must satisfy the associated dose constraint according to the clinical guidelines, so we adjust α_{oc}^{OAR} parameter in the CVaR constraint as described in (Romeijn et al. 2003) to meet this requirement. Let R-OAR stands for the rest of the corresponding OAR, then we use α_{oc}^{R-OAR}, which equals to $1-\frac{(1-\alpha_{oc}^{OAR})|V_o^{OAR}|-|V_o^{OAR}\setminus V_o^{R-OAR}|}{|V_o^{R-OAR}|}$, instead of α_{oc}^{OAR}. Clearly, if the set of voxels belonging also a TV is not empty, i.e. $|V_o^{OAR} \setminus V_o^{R-OAR}| \neq 0$, then $\alpha_{oc}^{R-OAR} > \alpha_{oc}^{OAR}$. Also, if $\alpha_{oc}^{R-OAR}|V_o^{R-OAR}|$ voxels satisfy the dose constraint in R-OAR then $\alpha_{oc}^{OAR}|V_o^{OAR}|$ voxels of the entire OAR also satisfy the constraint. Similarly, if a voxel belongs to more than one TV, it is considered only in the one with the highest prescription dose. Data sets provided by Istanbul University Oncology Institute include the rest of a structure if there is an intersection with this structure and a PTV. The rest of the structure is obtained by subtracting all voxels in the PTV with a margin of 2-3 mm.

Table 2. Properties of the prostate cancer data sets.

			Number of voxels of size 5 mm^3							
Patient	**m**	**n**	**PTV75.6**	**R-PTV56**	**Rectum**	**Bladder**	**PB**	**Lt F**	**Rt F**	**TOTAL**
P1	11	13	890	676	436	2836	58	1559	1476	7931
P2	9	13	1127	230	743	1567	20	923	953	5563
P3	9	13	1000	218	886	1915	53	1728	1791	7591
P4	9	13	889	407	736	2026	51	1653	1610	7372
P5	8	13	1056	346	632	755	90	2025	1845	6749
P6	12	9	1198	383	1035	4649	43	1300	1255	9863
P7	8	11	606	157	402	2911	67	1428	1495	7066
P8	9	9	699	213	757	4814	34	1827	1774	10118
P9	10	13	1971	219	753	1209	36	1630	1684	7502

Istanbul University Oncology Institute uses Varian's RapidArc technology to deliver VMAT treatment plans. The MLC system of the linear accelerator consists of 120 leaves, which are 0.5 cm thick at the isocenter for the central 20 cm, and 1 cm in the outer 2×10 cm. The maximum leaf speed is 2.5 cm/second and the dose rate can be 0-600 MU/minute. We set the associated parameters in our algorithm in alignment with these properties of the system. We assume that the gantry rotates at a constant rate and completes a tour in 6 minutes. There is one co-planar arc, thus delivery time of each plan is 6 minutes. The gantry moves from one control point to the consecutive one in 2 seconds, thus we set $\delta = 5$ beamlets. Moreover, the maximum radiation intensity (in MU) is 20 MUs since it is assumed that the radiation delivery lasts 2 seconds at a control point. The remaining parameters are as follows: lower and upper bound dose limits for PTV75.6 are set to 84 Gy (2.334 Gy per fraction) and 67 Gy (1.861 Gy per fraction), respectively, in accordance with the plans provided by the institute. Also, we set the upper bound dose limit for PTV56, which is 72 Gy (2 Gy per fraction). Finally, in CVaR parameter tuning operation we set ϵ_1 to 0.10 Gy and ϵ_2 to 0.03 Gy, and the penalty costs γ_{tc}^{TV} and γ_{oc}^{OAR} are set to 3000 and 1000 for each TV and OAR, respectively. We implement the proposed algorithm in Python 2.7

programming language (Python 2015) and use Gurobi 8.0 as MILP solver (Gurobi 2018). All tests are carried out on a 64-bit PC with 3.20 GHz Intel(R) Core(TM) i5-6500 CPU and 8 GB of RAM. We set the number of threads of Gurobi solver to 4.

4.1. Results

In Istanbul University Oncology Institute, the VMAT plans of all patients are optimized using two full arcs on older versions of Eclipse TPS (v.8.9 and v.15.1, Varian (2018)) using 6 MV photon beams. In Table 3 total MUs and dosimetric results of all plans are provided. According to these results all VMAT plans satisfy all dose-volume constraints given in Table 1 (except the plan of patient 6, since it does not satisfy the first dose-volume constraint of rectum, which requires $D_{\%35} \leq 40$ Gy). Total radiation dose (sum of MUs of two arcs) of plans varies between 570 and 743 MUs with average 633.9 MUs. Table 4 provides dosimetric results of VMAT plans obtained by our column generation based heuristic algorithm. Almost all plans are optimized within 20 minutes (1200 seconds) with an average of 1020 seconds. It takes a little longer to optimize plan 3 and plan 6 (1227 and 1782 seconds, respectively). We first note that total radiation intensity decreases in almost all plans significantly (except plan 5). The amount of radiation dose varies between 366 and 689 MUs with an average of 494.4 MUs. The maximum reduction occurs for the plan of patient 7, which is 363 MUs (48.9%). The average decrease of all plans is approximately 139.5 MUs and the average percentage of reduction is 22.0%. By assuming that the dose-influence matrices obtained by AAA algorithm (Sievinen et al. 2005) and by the singular value decomposed pencil beam algorithm (Bortfeld et al. 1993) used in matRad are sufficiently close, we can say that our proposed model and solution algorithm can find high quality plans requiring significantly less radiation. We observe that the first dose-volume constraint of rectum is not satisfied in the plans of three patients (patient 1, 6 and 8). However, the maximum deviation from the tolerance dose, which is 40 Gy, is 2.4 Gy. Note also that if we decrease the radiation intensities at all control points by same ratio without violating partial-volume constraints of PTVs, then the resulting deviations will be less. For example, in plan 6 it is possible to reduce the radiation intensities at all control points to 97.73% of the original intensities. Therefore, 95% of R-PTV56 will receive 56 Gy and 95% of PTV75.6 will receive 76 Gy. The resulting plan almost satisfies all dose constraints of rectum ($D_{\%35}$ will be 40.07 Gy). By this way total MUs of the plan also decreases by around 9.6 MUs. Similarly, we can adjust plan 1 and plan 8, and reduce the $D_{\%35}$ of rectum to 41.4 Gy and 41.2 Gy, respectively. Note that one needs to exercise caution while shifting the plans, since such a shift may also reduce the minimum dose to PTVs and increase the risk of resulting in cold spots. Moreover, in four out of nine plans (patient 1, 2, 6, and 8) $D_{\%90}$ of PB is more than 15 Gy (the maximum is 27.4 Gy). Since the deviations are not excessive the plans are acceptable according to the oncologists and medical physicists at Istanbul University Oncology Institute as well as other dose prescription recommendations in the literature such as limiting $D_{\%70}$ and $D_{\%90}$ of PB to 70 Gy and 50 Gy, respectively (Roach III et al. 2010). Thus, we can say that our proposed algorithm is capable of optimizing high-quality VMAT plans with significantly less MUs in clinically reasonable times. Finally, we provide DVHs of patient 3 obtained by our algorithm (in Figure 4) and by Eclipse (in Figure 5). We observe that DVHs of the structures in Figure 5 are smoother than those in Figure 4. The main reason for this difference is the usage of a lower

voxel resolution in our experiments compared to Eclipse. Especially for small structures (such as penile bulb) the resulting number of voxels becomes small, which makes the corresponding DVH less smooth. However, we note that the DVHs generated by both approaches satisfy clinical prescriptions with only minor deviations as discussed above.

Table 3. Dosimetric results of the VMAT plans obtained by Eclipse.

		PTV75.6	**R-PTV56**	**Rectum**		**Bladder**		**PB**	**Lt F**	**Rt F**
Patient	**MU**	$\mathbf{D_{95\%}}$	$\mathbf{D_{95\%}}$	$\mathbf{D_{35\%}}$	$\mathbf{D_{17\%}}$	$\mathbf{D_{50\%}}$	$\mathbf{D_{25\%}}$	$\mathbf{D_{90\%}}$	$\mathbf{D_{10\%}}$	$\mathbf{D_{10\%}}$
P1	591	76.6	56.9	39.9	50.9	32.9	42.6	10.7	26.5	25.8
P2	575	75.8	56.2	38.9	52.9	31.7	57.3	10.5	38.1	37.0
P3	743	76.4	56.5	34.2	48.7	22.0	57.9	8.6	22.0	18.4
P4	659	76.8	57.1	37.2	54.1	30.7	55.3	14.1	35.0	34.2
P5	661	75.9	56.5	38.4	56.7	37.7	63.5	6.0	37.8	37.8
P6	570	76.1	56.8	**41.2**	53.7	16.2	26.4	14.4	36.2	32.9
P7	667	76.2	56.9	37.7	48.8	5.5	14.9	5.3	24.8	27.5
P8	625	76.4	56.6	33.8	49.1	4.5	16.8	11.1	26.0	30.8
P9	614	76.0	56.7	38.8	55.2	30.6	62.8	8.0	34.9	39.4

Table 4. Dosimetric results of the VMAT plans obtained by the new algorithm.

		PTV75.6	**R-PTV56**	**Rectum**		**Bladder**		**PB**	**Lt F**	**Rt F**
Patient	**MU**	$\mathbf{D_{95\%}}$	$\mathbf{D_{95\%}}$	$\mathbf{D_{35\%}}$	$\mathbf{D_{17\%}}$	$\mathbf{D_{50\%}}$	$\mathbf{D_{25\%}}$	$\mathbf{D_{90\%}}$	$\mathbf{D_{10\%}}$	$\mathbf{D_{10\%}}$
P1	526	76.7	57.3	**42.0**	51.0	27.2	46.3	24.3	40.9	43.9
P2	561	77.2	56.8	38.1	53.7	36.5	63.3	25.1	34.3	33.5
P3	380	76.4	56.9	36.1	50.8	34.7	64.6	12.1	42.3	37.3
P4	523	77.1	57.2	37.2	48.9	34.2	64.3	14.2	45.1	48.0
P5	689	76.2	58.2	38.9	57.5	39.1	64.6	6.7	41.1	43.5
P6	424	77.8	57.3	**41.0**	57.8	7.4	27.8	20.4	46.2	45.8
P7	366	76.2	57.1	38.3	50.9	3.3	16.9	7.4	35.1	36.1
P8	509	77.8	58.0	**42.4**	61.3	6.4	25.8	27.4	26.5	22.5
P9	472	75.9	57.1	34.9	54.0	37.8	64.5	12.8	46.7	46.8

4.2. Sensitivity analysis on initial columns and tuning of CVaR constraints

In our next experiment, we analyze the effect of starting with the initial columns generated from the fluence maps obtained by solving M-VMATP model, and tuning the right hand side values of CVaR constraints.

We generate VMAT plans for all patients using two different sets of initial columns: the columns generated from a full treatment arc with maximum number of open beamlets, and from a randomly generated full treatment arc. These new initial columns are also feasible with respect to the MLC constraints (i.e. satisfying the consecutive ones property and the leaf motion limitations). Also, random columns are generated from a treatment plan satisfying the full volume constraints of all target voxels, which is obtained by solving a model including all geometry constraints and full volume constraints. According to our computational experiments, none of the resulting plans are clinically acceptable. In particular, the partial volume constraints of PTV75.6 or some of the

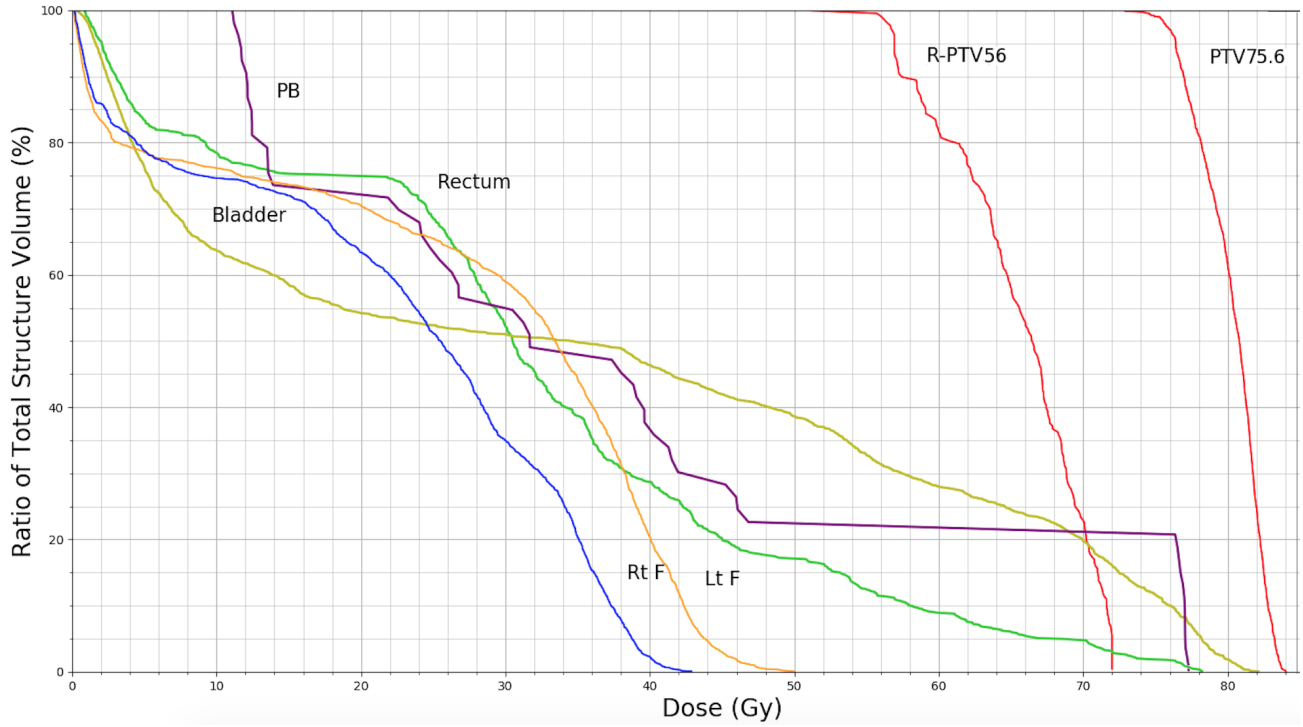

Figure 4. DVH of the plan of patient 3 obtained by our algorithm with full single arc.

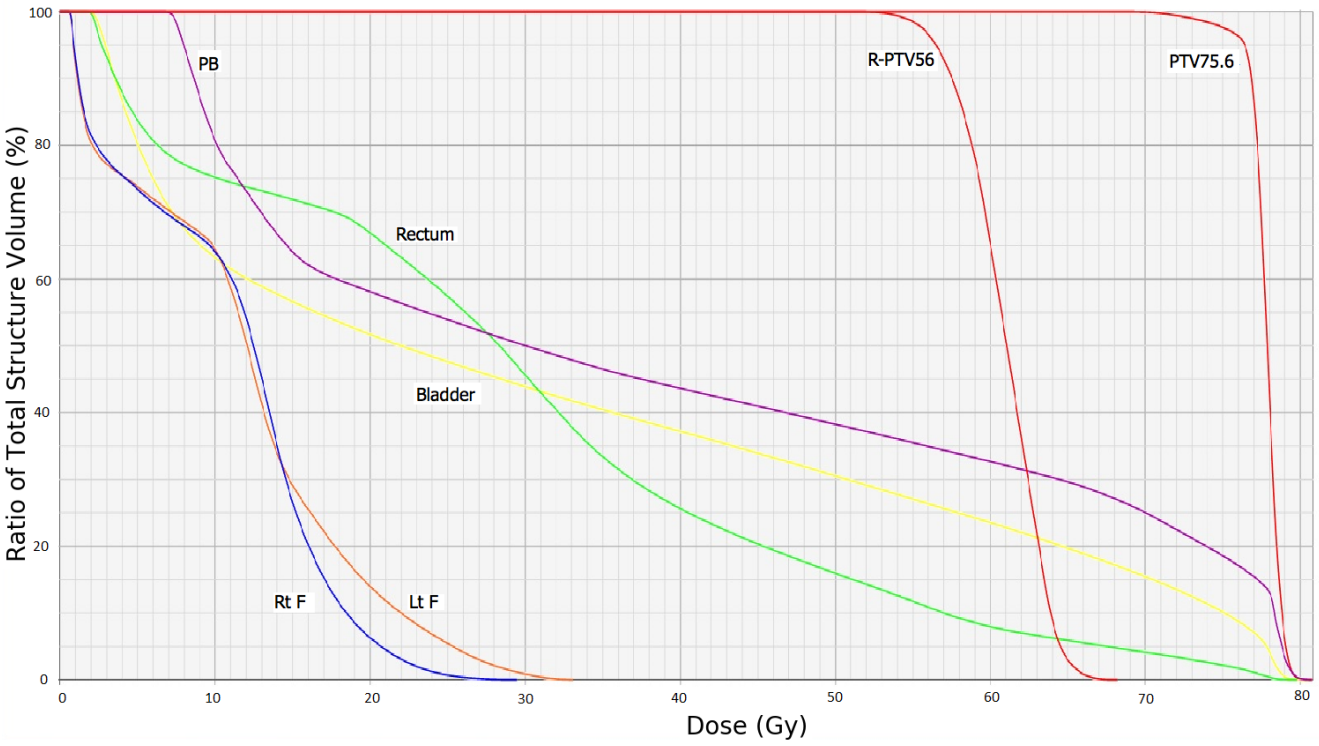

Figure 5. DVH of the plan of patient 3 obtained by Eclipse v.15.1 with full double arcs.

OARs are not satisfied. This implies that starting with initial columns generated from the fluence maps improves the quality of the plans in terms of dose distributions.

In our experiments, the average necessary time for the CVaR parameter tuning operation is 138.5 seconds. We repeat the computational experiments for all patients without this operation in order to see the effect on the performance of the algorithm. We observe from the results that the average CPU time of the plans without tuning operation decreases as expected. However, the average MUs of the plans increases by 76.4 MUs. In the new plans, rectum, bladder and penile bulb absorb less radiation. However, there are 3 plans where the partial-volume constraint of PTV75.6 is not satisfied. Therefore, tuning the right hand side parameters of CVaR constraints makes the resulting plans more reasonable without compromising OAR partial-volume constraints; and all PTV constraints are satisfied with fewer MUs (with an average decrease of 13.3%).

4.3. Computational results for CORT dataset

In our final experiment, we compare our proposed two-stage heuristic with the exact Benders decomposition algorithm in our previous work (Dursun et al. 2019*a*). In this experiment, we solved all instances used in our previous work (Dursun et al. 2019*a*) by our two-phase heuristic. Recall that the first phase of our heuristic algorithm tunes the tolerance doses of OARs, thus we have performed the computational experiments for both with and without the tuning operation. There are 11 different samples in dataset, and each one of them includes 5 different instances. Also, there is one target volume (TV) and one OAR. In Table 5, we give the summary results of all samples solved by the Improved Benders Algorithm 2, which is the best algorithm in Dursun et al. (2019*a*), and by our new two-phase heuristic. Note that we do not obtain a lower bound when we solve an instance by the two-phase heuristic, thus we use the lower bounds provided by Improved Benders Algorithm 2 in order to calculate optimality gaps. Also note that when we perform the tuning operation, the tolerance dose of OAR may increase, namely the problem may be simplified, thus the lower bound of the resulting model may decrease. Nevertheless, we used the same lower bound obtained by the Improved Benders Algorithm 2 to give an indication of optimality gaps. According to the results, CPU times and average optimality gaps obtained by our proposed two-phase heuristic are significantly smaller than those obtained by Improved Benders Algorithm 2. In both cases, the average necessary CPU time is around one minute (65.5 and 72.2 seconds for the computational experiments without tuning and with tuning operation, respectively). Two-phase heuristic can find a feasible solution with small optimality gap for all instances in both cases, however, it can solve only 2 and 6 out of 55 instances optimally. We should also note that in the resulting dose distributions of all instances when they are solved by the two-phase heuristic with tuning operation, partial-volume constraint of OAR is satisfied.

4.4. Discussion

VMAT plans are made by experienced dosimetrists in treatment planning departments. The planning process involves various manual interventions such as adapting planning objectives and constraints according to the individual anatomy of the patient. For example, shape and size of the tumor(s), and location of organs at risk are some of the anatomical properties that play an

Table 5. Summary results for CORT dataset (CPU in seconds, GAP %)

	Impr. Benders Alg. 2				Two-phase without CVaR Tuning				Two-phase with CVaR Tuning			
SAMPLE	GAP	CPU	S/T	O/T	GAP	CPU	S/T	O/T	GAP	CPU	S/T	O/T
22	0.00	112.2	5/5	5/5	3.09	30.1	5/5	0/5	2.86	28.9	5/5	0/5
44	0.00	627.8	5/5	5/5	0.30	29.0	5/5	0/5	0.46	29.3	5/5	0/5
66	0.14	1884.2	5/5	3/5	4.69	31.6	5/5	0/5	4.75	39.7	5/5	0/5
88	0.00	826.9	5/5	4/5	3.61	49.7	5/5	0/5	2.38	47.7	5/5	0/5
220	0.02	1187.1	5/5	4/5	4.01	31.8	5/5	0/5	2.48	39.6	5/5	0/5
660	0.22	3585.9	5/5	1/5	0.04	53.6	5/5	0/5	0.05	56.1	5/5	1/5
880	3.23	3600	5/5	0/5	0.07	66.8	5/5	1/5	0.09	68.0	5/5	1/5
1100	0.96	3600	5/5	0/5	0.06	79.0	5/5	1/5	0.06	90.3	5/5	2/5
1301	0.34	3600	5/5	0/5	0.16	96.6	5/5	0/5	0.08	112.8	5/5	0/5
1501	18.43	3600	4/5	0/5	0.18	120.6	5/5	0/5	0.12	127.1	5/5	1/5
1701	0.49	3600	5/5	0/5	0.18	131.6	5/5	0/5	0.07	154.8	5/5	1/5
Avg/Sum	**4.82**	**2483.4**	**54/55**	**21/55**	**1.49**	**65.5**	**55/55**	**2/55**	**1.22**	**72.2**	**55/55**	**6/55**

important role in the manual adjustments of the parameters, which influence the plan quality. In particular, dosimetrists try to guide the TPS towards a favorable plan by modifying optimization parameters. Thus, this manual process necessitates additional optimization steps and extra time, and also the quality of the final plan depends on the skills and experience of the dosimetrist as well as the complexity of the case and time allocated for planning. The VMAT plans whose dosimetric results are shown in Table 3 are obtained and adjusted by an experienced dosimetrist via a manual process as explained above. In the original data sets there are some additional structures (e.g. a subset of rectum) for which the dosimetrist defines additional constraints (in 7 out of 9 plans) to ensure that the related received radiation amounts fall into approvable limits. However, we do not use such an additional structure and/or additional dose-constraint in our algorithm. Our algorithm automatically adjusts parameters for each patient, and does not require any expert guidance.

5. Conclusions

In this study we provide a two-phase column generation based heuristic algorithm to solve a mixed integer linear programming (MILP) model for VMAT planning, which includes all dose-volume constraints and minimizes total radiation intensity delivered to the patient. Our proposed algorithm can find high quality VMAT treatment plans for problems with clinically adequate voxel and bixel (beamlet) resolution. In the first phase of the algorithm we generate an initial plan by solving a relaxed model, which is derived from the original model and gives a number of fluence maps. Then we convert these fluence maps into deliverable apertures and sequence them on an arc by applying a simple sequencing operation. In the second phase, we improve the initial solution by column generation iterations. Unfortunately, formulating VMAT planning problem results in a large-scale nonconvex optimization model due to the continuous nature of the problem. In order to avoid nonlinearities, we discretize a full arc into a large number of control

points and assume that the gantry rotates at a constant speed. Also, we use CVaR constraints to formulate dose-volume restrictions and an automated strategy for parameter tuning. We test our algorithm on nine real prostate patient data and compare the resulting VMAT plans with the ones obtained by an expert dosimetrist on Eclipse in one of the major oncology institutes of Turkey. Our model includes dose-volume constraints of all critical organs and two planning target volumes, parallel to clinical application. The results show that our algorithm is capable of finding plans of high quality with respect to clinical dose-volume criteria and requiring fewer MUs in clinically acceptable time. We only consider the consecutive ones property of MLC leaves in VMATP and the current network model does not consider connectedness property and allows interdigitation of the leaves. A potential future research direction is to extend the current network model to account for different MLC leaf constraints. Moreover, we assume that the gantry rotates at a constant speed, which may cause longer treatment time. Another potential future extension is to adjust the model to consider dynamic gantry speed in order to obtain higher quality treatment plans requiring less treatment time.

Acknowledgments

This research has been partially supported by the Boğaziçi University Research Fund with grant number 11520-16A03D1 and by the Turkish Directorate of Strategy and Budget under the TAM Project number DPT2007K120610.

References

Akartunalı, K., Mak-Hau, V. & Tran, T. (2015), 'A unified mixed-integer programming model for simultaneous fluence weight and aperture optimization in VMAT, Tomotherapy, and Cyberknife', *Computers & Operations Research* **56**, 134–150.

Bedford, J. L. (2009), 'Treatment planning for volumetric modulated arc therapy', *Medical Physics* **36**(11), 5128–5138.

Bellman, R. (1952), 'On the theory of dynamic programming', *Proceedings of the National Academy of Sciences* **38**(8), 716–719.

Boland, N., Hamacher, H. W. & Lenzen, F. (2004), 'Minimizing beam-on time in cancer radiation treatment using multileaf collimators', *Networks* **43**(4), 226–240.

Bortfeld, T., Schlegel, W. & Rhein, B. (1993), 'Decomposition of pencil beam kernels for fast dose calculations in three-dimensional treatment planning', *Medical Physics* **20**(2), 311–318.

Breedveld, S., Craft, D., van Haveren, R. & Heijmen, B. (2018), 'Multi-criteria optimisation and decision-making in radiotherapy', *European Journal of Operational Research* .

Buyyounouski, M. K., Horwitz, E. M., Price, R. A., Feigenberg, S. J. & Pollack, A. (2006), Prostate IMRT, *in* 'Image-Guided IMRT', Springer, pp. 391–410.

Bzdusek, K., Friberger, H., Eriksson, K., Hårdemark, B., Robinson, D. & Kaus, M. (2009), 'Development and evaluation of an efficient approach to volumetric arc therapy planning', *Medical Physics* **36**(6), 2328–2339.

Cambazard, H., O'Mahony, E. & O'Sullivan, B. (2012), 'A shortest path-based approach to the multileaf collimator sequencing problem', *Discrete Applied Mathematics* **160**(1), 81–99.

Cao, D., Afghan, M. K., Ye, J., Chen, F. & Shepard, D. M. (2009), 'A generalized inverse planning tool for volumetric-modulated arc therapy', *Physics in Medicine and Biology* **54**(21), 6725–6738.

Cedric, X. Y. & Tang, G. (2011), 'Intensity-modulated arc therapy: principles, technologies and clinical implementation', *Physics in Medicine and Biology* **56**(5), R31.

Christiansen, E., Heath, E. & Xu, T. (2018), 'Continuous aperture dose calculation and optimization for volumetric modulated arc therapy', *Physics in Medicine and Biology* **63**(21), 21NT01.

Craft, D., McQuaid, D., Wala, J., Chen, W., Salari, E. & Bortfeld, T. (2012), 'Multicriteria VMAT optimization', *Medical Physics* **39**(2), 686–696.

Dursun, P., Taşkın, Z. C. & Altınel, İ. K. (2016), Mathematical models for optimal volumetric modulated arc therapy (VMAT) treatment planning, *in* 'Procedia Computer Science (Proceedings of International Conference on Health and Social Care Information Systems and Technologies, HCist, Porto)', Vol. 100, pp. 644–651.

Dursun, P., Taşkın, Z. C. & Altınel, İ. K. (2019*a*), 'The determination of optimal treatment plans for Volumetric Modulated Arc Therapy (VMAT)', *European Journal of Operational Research* **272**(1), 372–388.

Dursun, P., Taşkın, Z. C. & Altınel, İ. K. (2019*b*), 'Using branch-and-price to determine optimal treatment plans for volumetric modulated arc therapy (vmat)', *Computers & Operations Research* **110**, 1–17.

Gören, M. & Taşkın, Z. C. (2015), 'A column generation approach for evaluating delivery efficiencies of collimator technologies in IMRT treatment planning', *Physics in Medicine and Biology* **60**(5), 1989.

Gozbasi, H. O. (2010), Optimization approaches for planning external beam radiotherapy, PhD thesis, Georgia Institute of Technology.

Gurobi, O. (2018), 'Gurobi optimizer reference manual version 8.0'. Accessed: 2019-01-08.
URL: *http://www.gurobi.com/documentation/8.0/refman.pdf*

Hall, E. J. & Wuu, C.-S. (2003), 'Radiation-induced second cancers: the impact of 3D-CRT and IMRT', *International Journal of Radiation Oncology Biology Physics* **56**(1), 83–88.

Hindi, H. (2013), A tutorial on optimization methods for cancer radiation treatment planning, *in* 'American Control Conference (ACC), 2013', IEEE, pp. 6804–6816.

Hoegele, W., Loeschel, R., Merkle, N. & Zygmanski, P. (2012), 'An efficient inverse radiotherapy planning method for VMAT using quadratic programming optimization', *Medical Physics* **39**(1), 444–454.

Luan, S., Wang, C., Cao, D., Chen, D. Z., Shepard, D. M. & Cedric, X. Y. (2008), 'Leaf-sequencing for intensity-modulated arc therapy using graph algorithms', *Medical Physics* **35**(1), 61–69.

Lyu, Q., Victoria, Y. Y., Ruan, D., Neph, R., O'Connor, D. & Sheng, K. (2018), 'A novel optimization framework for VMAT with dynamic gantry couch rotation', *Physics in Medicine and Biology* .

Mahnam, M., Gendreau, M., Lahrichi, N. & Rousseau, L.-M. (2017), 'Simultaneous delivery time and aperture shape optimization for the volumetric-modulated arc therapy (VMAT) treatment planning problem', *Physics in Medicine and Biology* **62**(14), 5589–5611.

Mahnam, M., Gendreau, M., Lahrichi, N. & Rousseau, L.-M. (2019), 'Integrating dvh criteria into a column generation algorithm for VMAT treatment planning', *Physics in Medicine & Biology* **64**(8), 085008.

MATLAB (2015), 'Version 8.5', *The MathWorks Inc* .

McCormick, G. P. (1976), 'Computability of global solutions to factorable nonconvex programs: Part iconvex underestimating problems', *Mathematical Programming* **10**(1), 147–175.

Men, C., Romeijn, H. E., Jia, X. & Jiang, S. B. (2010), 'Ultrafast treatment plan optimization for volumetric modulated arc therapy (VMAT)', *Medical Physics* **37**(11), 5787–5791.

Otto, K. (2008), 'Volumetric modulated arc therapy: IMRT in a single gantry arc', *Medical Physics* **35**(1), 310–317.

Palma, D., Vollans, E., James, K., Nakano, S., Moiseenko, V., Shaffer, R., McKenzie, M., Morris, J. & Otto, K. (2008), 'Volumetric modulated arc therapy for delivery of prostate radiotherapy: comparison with intensity-modulated radiotherapy and three-dimensional conformal radiotherapy', *International Journal of Radiation Oncology Biology Physics* **72**(4), 996–1001.

Papp, D. & Unkelbach, J. (2014), 'Direct leaf trajectory optimization for volumetric modulated arc therapy planning with sliding window delivery', *Medical Physics* **41**(1), 011701.

Peng, F., Jia, X., Gu, X., Epelman, M. A., Romeijn, H. E. & Jiang, S. B. (2012), 'A new column-generation-based algorithm for VMAT treatment plan optimization', *Physics in Medicine and Biology* **57**(14), 4569–4588.

Peng, F., Jiang, S. B., Romeijn, H. E. & Epelman, M. A. (2015), 'VMATc: VMAT with constant gantry speed and dose rate', *Physics in Medicine and Biology* **60**(7), 2955.

Pianykh, O. S. (2009), *Digital imaging and communications in medicine (DICOM): a practical introduction and survival guide*, Springer Science & Business Media.

Python (2015), 'Python 2.7.11 documentation'. Accessed: 2019-01-08.
URL: *https://docs.python.org/release/2.7.11/*

Roach III, M., Nam, J., Gagliardi, G., El Naqa, I., Deasy, J. O. & Marks, L. B. (2010), 'Radiation dose–volume effects and the penile bulb', *International Journal of Radiation Oncology Biology Physics* **76**(3), S130–S134.

Rockafellar, R. T., Uryasev, S. et al. (2000), 'Optimization of conditional value-at-risk', *Journal of Risk* **2**, 21–42.

Romeijn, H. E., Ahuja, R. K., Dempsey, J. F. & Kumar, A. (2006), 'A new linear programming approach to radiation therapy treatment planning problems', *Operations Research* **54**(2), 201–216.

Romeijn, H. E., Ahuja, R. K., Dempsey, J. F., Kumar, A. & Li, J. G. (2003), 'A novel linear programming approach to fluence map optimization for intensity modulated radiation therapy treatment planning', *Physics in Medicine and Biology* **48**(21), 3521.

Salari, E., Wala, J. & Craft, D. (2012), 'Exploring trade-offs between VMAT dose quality and delivery efficiency using a network optimization approach', *Physics in Medicine and Biology* **57**(17), 5587–5600.

Sievinen, J., Ulmer, W. & Kaissl, W. (2005), 'AAA photon dose calculation model in Eclipse', *Palo Alto (CA): Varian Medical Systems* **118**, 2894.

Smyth, G., Bamber, J. C., Evans, P. M. & Bedford, J. L. (2013), 'Trajectory optimization for dynamic couch rotation during volumetric modulated arc radiotherapy', *Physics in Medicine and Biology* **58**(22), 8163–8177.

Song, J., Shi, Z., Sun, B. & Shi, L. (2015), 'Treatment planning for volumetric-modulated arc therapy: Model and heuristic algorithms', *IEEE Transactions on Automation Science and Engineering* **12**(1), 116–126.

Teoh, M., Clark, C. H., Wood, K., Whitaker, S. & Nisbet, A. (2011), 'Volumetric modulated arc therapy: a review of current literature and clinical use in practice', *The British Journal of Radiology* **84**, 967–996.

Unkelbach, J., Bortfeld, T., Craft, D., Alber, M., Bangert, M., Bokrantz, R., Chen, D., Li, R., Xing, L., Men, C. et al. (2015), 'Optimization approaches to volumetric modulated arc therapy planning', *Medical Physics* **42**(3), 1367–1377.

Varian (2018), 'Eclipse treatment planning system'. Accessed: 2019-01-08.
URL: *https://www.varian.com/oncology/products/software/treatment-planning/eclipse-treatment-planning-system*

Wala, J., Salari, E., Chen, W. & Craft, D. (2012), 'Optimal partial-arcs in VMAT treatment planning', *Physics in Medicine and Biology* **57**(18), 5861–5874.

Wang, C., Luan, S., Tang, G., Chen, D. Z., Earl, M. A. & Cedric, X. Y. (2008), 'Arc-modulated radiation therapy (AMRT): a single-arc form of intensity-modulated arc therapy', *Physics in Medicine and Biology* **53**(22), 6291–6303.

Wieser, H.-P., Cisternas, E., Wahl, N., Ulrich, S., Stadler, A., Mescher, H., Mller, L.-R., Klinge, T., Gabrys, H., Burigo, L., Mairani, A., Ecker, S., Ackermann, B., Ellerbrock, M., Parodi, K., Jkel, O. & Bangert, M. (2017), 'Development of the open-source dose calculation and optimization toolkit matrad', *Medical Physics* **44**(6), 2556–2568.

Yan, H., Dai, J.-R. & Li, Y.-X. (2018), 'A fast optimization approach for treatment planning of volumetric modulated arc therapy', *Radiation Oncology* **13**(1), 101.

Yu, C. X. (1995), 'Intensity-modulated arc therapy with dynamic multileaf collimation: an alternative to tomotherapy', *Physics in Medicine and Biology* **40**(9), 1435–1449.